HHS Public Access

Author manuscript

Biosens Bioelectron. Author manuscript; available in PMC 2025 April 01.

Published in final edited form as:

Biosens Bioelectron. 2024 April 01; 249: 116017. doi:10.1016/j.bios.2024.116017.

Evaluation of restriction and Cas endonuclease kinetics using matrix-insensitive magnetic biosensors

Jisoo Im[a,b], **Songeun Kim**[a,b], **Suhyeon Park**[a,b], **Shan X. Wang**[c,d], **Jung-Rok Lee**[a,b,*]

[a]Division of Mechanical and Biomedical Engineering, Ewha Womans University, Seoul 03760, Republic of Korea

[b]Graduate Program in Smart Factory, Ewha Womans University, Seoul 03760, Republic of Korea

[c]Department of Materials Science and Engineering, Stanford University, Stanford, CA 93405, USA

[d]Department of Electrical Engineering, Stanford University, Stanford, CA 93405, USA

Abstract

The enzymatic actions of endonucleases *in vivo* can be altered due to bound substrates and differences in local environments, including enzyme concentration, pH, salinity, ionic strength, and temperature. Thus, accurate estimation of enzymatic reactions *in vivo* using matrix-dependent methods in solution can be challenging. Here, we report a matrix-insensitive magnetic biosensing platform that enables the measurement of endonuclease activity under different conditions with varying pH, salinity, ionic strength, and temperature. Using biosensor arrays and orthogonal pairs of oligonucleotides, we quantitatively characterized the enzymatic activity of EcoRI under different buffer conditions and in the presence of inhibitors. To mimic a more physiological environment, we monitored the sequence-dependent star activity of EcoRI under unconventional conditions. Furthermore, enzymatic activity was measured in cell culture media, saliva, and serum. Last, we estimated the effective cleavage rates of Cas12a on anchored single-strand DNAs using this platform, which more closely resembles *in vivo* settings. This platform will facilitate precise characterization of restriction and Cas endonucleases under various conditions.

*Corresponding author (jungrok@ewha.ac.kr).

Declaration of interests

The authors declare that they have no known competing financial interests or personal relationships that could have appeared to influence the work reported in this paper.

CRediT authorship contribution statement

J.I.: Data curation, Software, Formal analysis, Investigation, Visualization, Writing – original draft. S.K.: Software, Formal analysis, Validation, Visualization. S.P.: Validation, Visualization. S.X.W: Resources, Funding acquisition, Writing – review & editing. J.R.L.: Conceptualization, Resources, Supervision, Funding acquisition, Methodology, Writing – original draft.

Keywords

Endonuclease; Kinetics; Magnetic biosensors; Surface Michaelis–Menten; Giant magnetoresistance; Cas12a

1. Introduction

Recombinant DNA techniques employing restriction endonucleases have revolutionized biotechnology and medicine (Alberts 2003), and have facilitated the synthesis of a plethora of valuable proteins for medication (Kinch 2015). Recent advances in these technologies have extended their capabilities to *in vivo* gene editing, thereby opening a new era of human genome editing (Doudna 2020). Since understanding pharmacodynamics is of paramount importance during drug development, it is essential to thoroughly characterize the endonucleases used in medications to optimize delivery strategies, tailor drug concentrations, and mitigate potential side effects (van Haasteren et al. 2020). Traditionally, the kinetics of endonuclease has been assessed using optical techniques such as fluorescence resonance energy transfer (FRET) (Huyke et al. 2022) in a test tube where enzymes and substrates are present in a free-floating state. However, the *in vivo* context of gene editing would significantly differ from controlled *in vitro* conditions. The endonucleases should be limited in their quantities to minimize undesirable side effects, and their target DNA substrates are restricted in both number and location, being anchored in chromatin or in the nucleus. Despite the relatively higher abundance of endonucleases compared to substrates, the presence of surface-bound substrates in minute quantities can lead to deviations in reaction kinetics from the classic Michaelis–Menten model (Anne and Demaille 2012). More importantly, conventional measurements of enzyme kinetics rely heavily on fluorescence, which is affected by pH and temperature (Wurth et al. 2013). Consequently, it would be difficult to decouple the signal of cleavage from pH- or temperature-induced artifacts when measuring reaction rates under various physiological conditions. Furthermore, the photobleaching of fluorescent dyes poses an inevitable challenge to continuous monitoring of the progression curve of enzyme actions. This monitoring is, however, a crucial requirement for obtaining effective kinetic parameters from surface Michaelis–Menten models, and is particularly relevant for describing the enzymatic kinetics of surface-bound substrates (Anne and Demaille 2012).

Numerous studies have sought to precisely evaluate the kinetics of endonucleases under diverse conditions, yet they have faced challenges in simultaneously exploring the full range of parameters involved, which include pH, salinity, ionic strength, and temperature (Davidi et al. 2016). One of the notable approaches to measuring endonuclease kinetics involves the use of electrochemical sensors (Cui et al. 2024; Gao et al. 2017). However, studies employing electrochemical methods have explored only a limited number of parameters so far. Given that electrochemical sensors rely on detecting changes in electrical properties, which may be affected by pH and salinity, magnetic sensors could be a promising alternative for investigating endonuclease kinetics under charge-varying environments. Thus, we here report a magnetic sensing platform that facilitates accurate evaluation of endonuclease kinetic parameters under various conditions. The magnetic biosensors implemented in this

platform are based on the quantum mechanical effect of giant magnetoresistance (GMR) and can detect a minute magnetic field created by magnetic nanoparticles (MNPs) in real time (Lee et al. 2016). By monitoring the release of MNPs attached to oligonucleotides on the sensor surface when endonucleases cleave restricted sites on oligonucleotides, GMR biosensors can measure enzyme kinetics. In addition, the GMR biosensors have demonstrated insensitivity to numerous matrices, including human bodily fluids (Gaster et al. 2009; Lee et al. 2016), and their signals can be corrected to eliminate temperature artifacts (Kim et al. 2023). Since GMR biosensors have been fabricated in an array of sensors on a chip to measure multiple analytes in a sample with individual sensors (Lee et al. 2018), endonucleases can be screened simultaneously against multiple oligonucleotides including both their on- and off-target sequences.

In this work, we chose EcoRI as a model system to conduct a precise evaluation of endonuclease kinetic parameters under various conditions. To monitor sequence-dependent enzyme reactions, orthogonal pairs of oligonucleotides were carefully designed by incorporating both on- and off-target sequences into pre-screened orthogonal barcode sets (Xu et al. 2009). Furthermore, the platform was used to estimate the effective kinetic parameters of Cas12a in cleaving single-stranded DNAs (ssDNAs).

2. Materials and Methods

2.1 Preparation of the magnetic biosensor

The magnetic biosensor chip was fabricated as described previously (Kim et al. 2022). Amino-modified oligonucleotides were pre-synthesized as probe DNAs by Integrated DNA Technologies (USA) and were diluted to 50 μM in 2× saline-sodium citrate (SSC). Probe DNAs were spotted on the different sensors by a robotic arrayer (SciFlexArrayer S3, Scienion, Germany). In addition, 1 % bovine serum albumin (BSA) and biotinylated BSA were deposited on different sensors. After overnight incubation at 4 °C, the sensor chip was assembled into a custom-made cartridge. The sensor chip was washed with a washing buffer (phosphate-buffered saline with 0.1 % BSA and 0.05 % Tween-20), and then blocked with 1 % BSA for 1 h. Finally, the chip was washed sequentially with the washing buffer and the 2× SSC buffer before being used for subsequent assays.

2.2 Orthogonality of DNA pairs

Biotinylated oligonucleotides (target DNAs) complementary to respective probe DNAs immobilized on the sensors were obtained from Integrated DNA Technologies. Only one type of target DNA was diluted to 500 nM in 2× SSC buffer, added to the prepared magnetic biosensor chip, and incubated at 37 °C for 1 h on a shaker. The chips were then washed with 2× SSC buffer, and inserted into custom-made reader stations. Signal baselines were recorded at 37 °C and then 65 μL of streptavidin-coated MNPs (Miltenyi Biotec, Germany) were added to the chips until the signals were saturated. The obtained signals were all referenced to the average signal of the BSA-coated sensors.

2.3 Enzyme preparation

EcoRI (ThermoFisher, ER0271) at 10 U μL^{-1} was diluted to 1 U μL^{-1} (unless otherwise indicated) using the buffer provided by the manufacturer or in a custom-made buffer solution. The commercial EcoRI buffer contains 50 mM Tris-HCl (pH 7.5), 10 mM $MgCl_2$, 100 mM NaCl, 0.02 % TritonX-100, and 0.1 mg mL^{-1} BSA. The custom-made buffer solutions include buffers with different concentrations of NaCl (10, 20, 50, and 100 mM), Tris-HCl (10, 20, 50, and 100 mM), and ethylenediaminetetraacetic acid (EDTA, 0.01, 0.1, 1, and 10 mM) as well as buffers in Tris-HCl pH 7.5 and pH 8.0.

2.4 Enzyme kinetics assays

The target DNAs were mixed together and diluted to the final concentrations of 500 nM in 2× SSC buffer, and 100 μL of this mixture was added to the prepared magnetic biosensor chip to initiate hybridization with DNA probes at 37 °C for 1 h on a shaker. The chip was then cooled down and washed with 2× SSC buffer. Next, the chip was plugged into a custom-made reader station at 37 °C (unless otherwise indicated). After signal baselines were recorded, 65 μL of MNPs were added to the reaction well. After the signals were saturated, the temperature was dropped to 20 °C, and the chip was washed with a solution containing 10 mM NaCl to remove unbound MNPs while stabilizing the DNA hybrids. Next, the temperature was increased again to 37 °C, and 100 μL of an enzyme solution was added to the reaction well.

2.5 Buffer preparation for star activity tests

For the effects of different metal ions, buffer solutions with different metal ions were prepared in 10 mM Tris-HCl (pH 7.5) using $MgCl_2$, $MnCl_2$, and $CaCl_2$. The final concentrations of $MgCl_2$, $MnCl_2$, and $CaCl_2$ in the buffer solutions were 10 mM, 2 mM, and 5 mM, respectively. For the pH effect of star activity, two kinds of buffer solutions with $MnCl_2$ at 2 mM were prepared in either 10 mM Tris-HCl pH 7.5 or 8.0. To monitor star activity under different salinity and ionic strengths, 2 mM $MnCl_2$ buffer solutions were prepared with different concentrations of NaCl (10, 20, 50, and 100 mM) in 10 mM Tris-HCl pH 7.5 or different concentrations of Tris-HCl pH 7.5 (10, 20, 50, and 100 mM) in the absence of NaCl.

2.6 Calculation of kinetic parameters

To obtain k_{eff} values, a curve fitting algorithm was developed using non-linear regression algorithms implemented in MATLAB (MathWorks, USA). Data points from the first 15 min (30 min for star activity analyses due to slow reaction kinetics) immediately after the enzyme injection were taken from all recordings, referenced to the average signal of BSA-coated sensors, and normalized to the value at the enzyme injection to fit the mathematical model, $y = \frac{1-c}{2}\left\{(1+a)e^{-\frac{b(a-1)}{2a}t} + (1-a)e^{-\frac{b(a+1)}{2a}t}\right\} + c$ with three fitting parameters, a, b, and c.

2.7 Kinetics assay with Cas12a

For Cas12a analyses, biotinylated DNA oligonucleotides were spotted on different sensors. Cas12a (*Lb* Cas12a or Cpf1) from *Lachnospiraceae bacterium* at 1 μM was obtained from New England Biolabs (M0653S; USA) and mixed with crRNA at 30 nM and BRCA1 target stands (TSs) obtained from Integrated DNA Technologies at 30 nM. Among the two different lengths of BRCA1 target stands used, the short TS (21 bp) was used for most experiments (the long TS was 45 bp). The final concentration of Cas12a in the mixture was 30 nM, and the reaction buffer provided by the manufacturer (10 mM Tris-HCl pH 7.9, 50 mM NaCl, 10 mM $MgCl_2$, and 0.1 mg mL^{-1} BSA) was used to prepare the mixture. For serum measurements, Cas12a, crRNA, and short TS were mixed in human serum (Merck, S1) with $MgCl_2$ at 10 mM. In addition to mixtures with reaction buffers, mixtures without each component were also prepared to assess the function of each component. Next, each mixture was incubated at 25 °C for 30 min. After binding signals of MNPs were saturated at 37 °C, unbound MNPs were washed away and each enzyme mixture was added to the reaction wells of different chips.

3. Results and Discussion

3.1 Magnetic biosensing platform for evaluating endonuclease kinetics

To readout signals from GMR-based magnetic biosensors and control their temperature, a custom-made reader station was equipped with data acquisition (DAQ) boards and a temperature controller as described previously (Kim et al. 2023) (Fig. 1a). An array of 80 GMR biosensors was fabricated on a chip, which was then mounted on a printed circuit board and assembled in a custom-made cartridge including a thermoelectric cooler (TEC) and a resistance temperature detector (RTD) (Fig. 1b). In addition, the upper part of the cartridge served as a reaction well over the sensors. Seven different probe DNAs containing potential cleavage sites of EcoRI (P1–P6) as well as a random sequence (NP), which served as a negative control, were immobilized on different GMR biosensors on a chip along with BSA (Table S1). Next, biotinylated target DNAs (T1–T6 and NT) that were complementary to the probe DNAs (Table S2) were added to the reaction well to produce DNA hybrids (Fig. 1c). After hybridization, streptavidin-coated MNPs were added and bound to the DNA hybrids (Fig. 1d). The underlying GMR biosensors then detected the magnetic field induced by the MNPs and generated signals that were proportional to the number of MNPs bound to the DNA hybrids. The GMR biosensor signals were typically reported as changes in the magnetoresistance ratio (ΔMR). The MR represents the ratio of changes in electrical resistance induced by an external magnetic field to the nominal resistance of the sensor. After the chip was washed to remove unbound MNPs, an EcoRI solution was introduced to the chip and the temperature was set to a desired level (Fig. 1e). As DNA hybrids with on-target sequences were cleaved by EcoRI, MNPs were released from the sensor surface, resulting a reduction in signal intensity (Fig. 1f and g). However, DNA hybrids with off-target sequences remained intact, keeping the number of MNPs near the sensor surface unchanged over time. Thus, the GMR biosensors showed unaffected signals (Fig. 1g). To realize cleavage events through the release of MNPs from the surface, it is crucial for the MNP size to be smaller than 100 nm to avoid precipitation but sufficiently large to produce higher signals (Kim et al. 2022; Wang et al. 2014). Therefore, the optimal diameter for

MNPs has been reported to be approximately 50 nm (Wang et al. 2014), and the MNPs used in this study have a diameter of 46 nm (Gaster et al. 2011). For enzyme kinetics, the most important kinetic parameters are the binding rate (k_1) and the unbinding rate (k_{-1}) between enzyme and substrate as well as the turnover number (k_{cat}), which denotes the number of converted substrates per unit time. To obtain these kinetic parameters for the EcoRI reaction, cleavage signals (or progress curve) were normalized by the signal at the point of enzyme addition. They were then fitted to a mathematical model shown as equation (1), which is slightly modified from the exact solution of surface enzyme kinetics reported by a previous study (Anne and Demaille 2012) (Fig. 1h and see details in the Supplementary Information).

$$S = \frac{1 - c}{2}\left\{(1+\lambda)e^{-\frac{\sigma(\lambda-1)}{2\lambda}t} + (1-\lambda)e^{-\frac{\sigma(\lambda+1)}{2\lambda}t}\right\} + c \quad (1)$$

where S is the normalized GMR biosensor signal and c is an offset variable, $\sigma = k_1[E]_t + k_{-1} + k_{cat}$, and $\lambda = 1/\sqrt{1 - 4k_1[E]_t k_{cat}/\sigma^2}$ with the total concentration of enzymes, $[E]_t$. Once the two variables σ and λ, were obtained through curve fitting analysis, the effective cleavage rate, k_{eff}, could be calculated using equation (2) to report a single-valued kinetic parameter for easy comparison across different experimental settings.

$$k_{eff} = \frac{k_{cat}}{1 + (K_M/[E]_t)} = k_{cat}\frac{[E]_t}{[E]_t + K_M} = \frac{\sigma\left(\lambda^2 - 1\right)}{4\lambda^2} \quad (2)$$

where Michaelis constant $K_M = (k_{cat} + k_{-1})/k_1$.

3.2 Characterization of EcoRI

We first characterized EcoRI, a well-studied type II restriction endonuclease (McClarin et al. 1986; Wright et al. 1999), as a model system. Interestingly, EcoRI can cleave non-canonical sequences (i.e., sequences other than its canonical sequence, GAATTC) under non-optimal conditions, allowing an investigation into sequence-dependent reactions under various conditions. To ensure that sequence-specific DNA hybrids formed on each sensor, orthogonal pairs of probe and target DNAs were designed to avoid any significant cross-hybridization and formation of homodimers based on thermodynamic properties (Tables S1, S2, and S3). Once hybridized, each DNA hybrid contained either canonical (P1 and T1) or non-canonical (P2–P6 and T2–T6) sequences of EcoRI as well as a random sequence as a negative control (NP and NT). To validate the orthogonality of the DNA pairs, each GMR biosensor chip was functionalized with seven different probes (P1–P6, and NP), and only one type of target DNA was added to each chip. These results confirmed that only matched pairs produced fairly high signals and that cross-hybridization did not occur (Fig. 2a).

We then performed enzyme assays with EcoRI to determine its optimal temperature and concentration using the buffer solution provided by the manufacturer (Fig. 2b and c). The optimal condition was found to be 1 U μL^{-1} of EcoRI at 37 °C, which is consistent with

previous studies (Terry et al. 1983) and accords with the manufacturer's recommendations. Interestingly, the enzymatic kinetics determined using this platform did not follow the classic Michaelis–Menten model. Instead, it followed a surface Michaelis–Menten model, as evidenced by the behavior of the effective cleavage rates at different enzyme concentrations (Fig. 2d), which was in good agreement with equation (2). Even when the observed cleavage rates were estimated by fitting data to a simple exponential function, $y = \exp(-k_o t)$, and plotting these versus the concentrations of the enzyme, the behavior followed equation (2), which again ensured that surface Michaelis–Menten model explained the kinetics on our platform well (Fig. S1). Next, two important kinetic parameters, k_{cat} and K_M, were estimated from fitted curve to be 0.9641 min^{-1} and 0.2183 U μL^{-1}, respectively (Fig. 2d). Moreover, the turnover number was in agreement with previously reported values under similar conditions (Wright et al. 1999), but Michaelis constant contrasted with other values reported in the literatures because the concentration of the enzyme was not provided in molar concentration. Furthermore, we tested our platform using another enzyme, EcoRV, which cleaves a palindromic sequence of GATATC. This endonuclease also showed a clear sequence-specific reaction and a fast cleavage rate of the target sequence (see details in the Supplementary Information and Fig. S2).

3.3 Evaluation of EcoRI kinetics under various conditions

Next, we further evaluated the kinetics of EcoRI under different environmental conditions, including varying salt concentrations, pH levels, ionic strengths, and in the presence of inhibitors. To investigate the effect of salinity, we tested buffers with varying concentrations of NaCl while keeping the concentrations of Tris-HCl and $MgCl_2$ the same as in the standard buffer provided by the manufacturer. Due to electrostatic interactions between the enzyme and substrate, lower NaCl concentrations were found to attenuate the enzymatic activity of EcoRI (Fig. 3a). To solely examine the influence of ionic strength, buffers with different concentrations of Tris-HCl (pH 7.5) were prepared with NaCl at 100 mM and $MgCl_2$ at 10 mM. Given that most enzymatic activities show characteristic optimal ionic strengths (Wright et al. 1999), the optimal concentration of Tris-HCl in EcoRI reaction was found to be 50 mM, which is consistent with the concentration present in the standard buffer provided by the manufacturer (Fig. 3b). We then tested the effect of pH on enzymatic activity between Tris-HCl pH 7.5 and 8.0 (Fig. 3c). As expected, no significant difference was observed as the typical pH range for the enzymatic reaction of EcoRI is between pH 7.2 and 8.6 (Woodhead et al. 1981). Mg^{2+} is a key cofactor for the enzymatic reaction, but enzymatic activity has been found to be relatively insensitive to Mg^{2+} concentration (Pingoud et al. 2009). Instead of varying the concentration of Mg^{2+}, we estimated enzyme kinetic parameters in the presence of an inhibitor, EDTA, which chelates Mg^{2+} and thereby deactivates the metal-dependent enzymatic activity of EcoRI. We found that effective cleavage rates were not significantly affected by varying concentrations of EDTA until it matched the concentration of Mg^{2+} in the buffer (10 mM), at which point the enzymatic reactions of EcoRI were completely quenched (Fig. 3d). Our platform not only enables the measurement of enzyme kinetics in pre-mixed buffers, but also facilitates real-time buffer modification and monitoring of its immediate effect on enzymatic activity (see another example in Fig. S3). We demonstrated this ability by stopping enzymatic digestion in the middle of the reaction via the addition of EDTA into the reaction well

(Fig. 3e). The comparison of normalized cleavage curves with and without real-time EDTA addition clearly revealed that the real-time addition of EDTA slowed down the enzymatic reaction, eventually quenching it (Fig. 3f).

3.4 Star activity of EcoRI

To demonstrate the multiplex capability of our platform, we examined sequence-dependent reactions of EcoRI. EcoRI is known to cleave at non-canonical DNA sequences that differ from GAATTC, which is referred to as EcoRI* (star) activity, under non-optimal buffer conditions (Pingoud and Jeltsch 1997; Pingoud et al. 2014). Following the hierarchical orders of non-canonical sequences for star activity (AAATTC > TAATTC > CAATTC, GGATTC > GTATTC) reported previously (Gardner et al. 1982; Pingoud et al. 2014), we named orthogonal DNA pairs, PT2 to PT6, in the same order (PT2 represents a hybrid between P2 and T2, and so on). In addition, it has been reported that a low salt concentration, high pH, or the presence of Mn^{2+} can induce the star activity of EcoRI (Pingoud et al. 2014; Polisky et al. 1975), but clear reaction conditions and sequence preferences regarding star activity have not yet been fully established. First, we evaluated the effect of divalent metal ions on star activity (Fig. 4a). Here, buffers contained only 10 mM Tris-HCl (pH 7.5) with either $MgCl_2$ at 10 mM, $MnCl_2$ at 2 mM, or $CaCl_2$ at 5 mM. Interestingly, the Mg^{2+}-based buffer still produced a higher cleavage rate on the canonical sequence, whereas the Mn^{2+}-based solution induced star activity on more non-canonical sequences without affecting the canonical one. Therefore, we used Mn^{2+}-based buffers for all subsequent experiments involving star activity to evaluate more sequence-dependent reactions. While Mn^{2+} is known to be involved in enzymatic reactions in the active site by interacting with water molecules, Ca^{2+} does not participate in the reaction even though its size is comparable to that of the magnesium ion (Mg^{2+}) (Pingoud et al. 2014). Consequently, no cleavage signals were observed with Ca^{2+}-based buffers (Fig. 4a). Next, to investigate how pH affects the star activity of EcoRI, another buffer containing 10 mM Tris-HCl (pH 8.0) and 2 mM $MnCl_2$ was tested in comparison with Tris-HCl (pH 7.5) (Fig. 4b). These results indicated that a higher pH leads to greater effective cleavage rates for both canonical and multiple non-canonical sequences. This finding is well agreed with previous studies reporting that the optimal pH for star activity is between 8.0 and 9.5 (Polisky et al. 1975). Next, we examined the effects of salinity and ionic strength on star activity and enzyme kinetics. Four different concentrations of NaCl with 10 mM Tris-HCl (pH 7.5) and 2 mM $MnCl_2$ were tested, and these results identified an optimal salinity for each sequence (Fig. 4c). For example, 50 mM NaCl was optimal for PT2 and PT3, while 20 mM NaCl was optimal for PT4. With respect to ionic strength, effective cleavage rates monotonically increased as the concentration of Tris-HCl (pH 7.5) was increased within the tested range from 10 to 100 mM without any salts (Fig. 4d). No cleavage signal was detected in any of the experiments for negative controls, DNA hybrids between NP and NT. Interestingly, the effective cleavage rate of EcoRI on PT3 was always higher than that on PT2, which was not consistent with the previous finding. This inconsistency was understood as reflecting the fact that the composition and pH of the buffer used in the present study significantly differed from previous studies (Gardner et al. 1982; Thielking et al. 1990). After thoroughly demonstrating the capability of our platform, we demonstrated that our platform is compatible with physiologically relevant liquids by measuring the

kinetic parameters of EcoRI in cell culture media, serum, and saliva (see details in the Supplementary Information and Figs. S3 and S4).

3.5 Cas12a kinetics

Last, we estimated the trans-cleavage rates of Cas12a on surface-bound ssDNAs because CRISPR-Cas systems are promising tools for genome editing and diagnostics (Hendel et al. 2015; Roh et al. 2023). To activate trans-cleavage of Cas12a, a DNA segment of TS and a complementary crRNA were mixed with Cas12a, and incubated to form Cas12a complexes (Fig. 5a and see details in the Supplementary Information). A sequence of TS was selected from the BRCA1 gene due to its association with an increased risk of ovarian and breast cancer, as well as its utility in diagnostics (Kuchenbaecker et al. 2017). A magnetic biosensor chip was functionalized with four different biotinylated ssDNAs (Table S4), and MNPs were then added to the chip (Fig. 5b). After signals were fully saturated, the activated Cas12a complexes were added to the chip, initiating cleavage of ssDNAs on the sensor surface (Fig. 5c and d). The ssDNAs on the sensors included different sequences, but the effective cleavage rates of Cas12a complexes on each of them were similar (Fig. 5e), confirming that Cas12a indiscriminately cleaves ssDNAs without any significant preference (Chen et al. 2018). In addition, the measured effective cleavage rates (0.2852 to 0.4232 min^{-1} with an average of 0.3438 min^{-1}) were fairly comparable to calculated values (0.45 to 0.76 min^{-1}). These calculated values were determined by taking the concentration of Cas12a complexes to be 30 nM and using the previously reported catalytic efficiency, k_{cat}/K_M, and the observed cleavage rate, $k_{cat} \cdot [E]_t/K_M$ (Ramachandran and Santiago 2021). To confirm that cleavage signals were produced by the Cas12a complexes, we performed experiments with buffers missing different reaction components (Cas12a, crRNA, or TS; Table S5). No cleavage signals were observed for any of these buffers (Fig. 5e). Furthermore, the effective cleavage rates of Cas12a were repeatedly measured to estimate the reproducibility of the measurement, and the inter-CV (coefficient of variation) was determined to be 12.5 % (Fig. S5). Interestingly, when Cas12a complexes were generated with a 45 bp TS complementary to the crRNA instead of the 21 bp TS used above (see the sequences in the Supplementary Information), the average effective cleavage rate was reduced by 40 % (Fig. 5f). We hypothesized that the extended tails of the long TS in the Cas12a complex may induce steric hindrance with the MNP or the sensor surface because the size of Cas12a is approximately 10 nm (Li et al. 2023) and is therefore comparable to the lengths of the biotinylated oligonucleotides used. Furthermore, we found that the effective cleavage rates of Cas12a in serum (average: 0.0360 min^{-1}) were significantly attenuated by a factor of 10 compared to those in the buffer (Fig. S6). This attenuation did not result from the blockage of cleavage sites due to specific or non-specific absorption of abundant proteins in serum onto the MNPs or sensor surfaces because pre-incubation with serum before adding Cas12a did not show any significant reduction in the effective cleavage rate (Fig. S7). Notably, the pH values of cell culture media, saliva, and serum used in this study were deviated from the optimal pH for Cas12a activity, and a significant attenuation in the effective cleavage rates of Cas12a was also observed in cell culture media and saliva (Fig. S8). Therefore, we propose that pH is the primary reason for this attenuation, as previous studies have reported a sharp drop in the efficiency of Cas12a cleavage away from its optimal pH (Cui et al. 2024; Rananaware et al. 2023).

4. Conclusions

We demonstrated that our magnetic biosensing platform can evaluate the effective cleavage rates of endonucleases on multiple sequences simultaneously under a variety of environmental conditions. The proximity-based nature of the sensing mechanism in the GMR biosensor with MNPs facilitated the precise monitoring of cleavage events, and the normalized cleavage signals represented the fraction of cleaved DNA hybrids well. Through curve fitting based on the surface Michaelis–Menten model, effective cleavage rates were estimated for a wide range of conditions and agreed well with previously reported equivalent values. To determine k_{cat} and K_M, the effective cleavage rates should be measured using varying concentrations of the enzyme or substrate, as demonstrated above. However, since environmental factors including temperature, pH, salinity, and ionic strength affect individual kinetic parameters separately, their combined effect on the enzymatic reaction is complicated and difficult to predict. Moreover, it would be time-consuming to perform multiple experiments to identify kinetic parameters under many different conditions. Thus, evaluating an effective cleavage rate that manifests the overall outcome may be of greater practical significance for the development of new endonuclease-based drugs or diagnostic tools.

Supplementary Material

Refer to Web version on PubMed Central for supplementary material.

Acknowledgments

This work was supported by the National Research Foundation of Korea (NRF) grants funded by the Korean government (NRF-2019M3C1B8090804, NRF-2019R1F1A1062638, NRF-2020R1C1C1005416, and NRF-2023R1A2C1006611) and the National Institutes of Health (NIH) grants (1R01CA257843 and 1R21DK131776).

References

Alberts B, 2003. Nature 421(6921), 431–435. [PubMed: 12540917]

Anne A, Demaille C, 2012. Langmuir 28(41), 14665–14671. [PubMed: 22978617]

Chen JS, Ma EB, Harrington LB, Da Costa M, Tian XR, Palefsky JM, Doudna JA, 2018. Science 360(6387), 436–439. [PubMed: 29449511]

Cui J, Luo Q, Wei C, Deng X, Liang H, Wei J, Gong Y, Tang Q, Zhang K, Liao X, 2024. Anal Chim Acta 1285, 342028. [PubMed: 38057050]

Davidi D, Noor E, Liebermeister W, Bar-Even A, Flamholz A, Tummler K, Barenholz U, Goldenfeld M, Shlomi T, Milo R, 2016. P Natl Acad Sci USA 113(12), 3401–3406.

Doudna JA, 2020. Nature 578(7794), 229–236. [PubMed: 32051598]

Gao X, Geng M, Li Y, Wang X, Yu H-Z, 2017. Anal Chem 89(4), 2464–2471. [PubMed: 28192924]

Gardner RC, Howarth AJ, Messing J, Shepherd RJ, 1982. DNA 1(2), 109–115. [PubMed: 6299666]

Gaster RS, Hall DA, Nielsen CH, Osterfeld SJ, Yu H, Mach KE, Wilson RJ, Murmann B, Liao JC, Gambhir SS, Wang SX, 2009. Nat Med 15(11), 1327–1332. [PubMed: 19820717]

Gaster RS, Xu L, Han S-J, Wilson RJ, Hall DA, Osterfeld SJ, Yu H, Wang SX, 2011. Nat Nanotechnol 6(5), 314–320. [PubMed: 21478869]

Hendel A, Bak RO, Clark JT, Kennedy AB, Ryan DE, Roy S, Steinfeld I, Lunstad BD, Kaiser RJ, Wilkens AB, Bacchetta R, Tsalenko A, Dellinger D, Bruhn L, Porteus MH, 2015. Nat Biotechnol 33(9), 985–989. [PubMed: 26121415]

Huyke DA, Ramachandran A, Bashkirov VI, Kotseroglou EK, Kotseroglou T, Santiago JG, 2022. Anal Chem 94(27), 9826–9834. [PubMed: 35759403]

Kim S, Kim J, Im J, Kim M, Kim T, Wang SX, Kim D, Lee JR, 2022. Microchim Acta 189(7), 256.

Kim S, Wang SX, Lee J-R, 2023. Biosens Bioelectron : X 14, 100356. [PubMed: 37799506]

Kinch MS, 2015. Drug Discov Today 20(4), 393–398. [PubMed: 25220442]

Kuchenbaecker KB, Hopper JL, Barnes DR, Phillips KA, Mooij TM, Roos-Blom MJ, Jervis S, van Leeuwen FE, Milne RL, Andrieu N, Goldgar DE, Terry MB, Rookus MA, Easton DF, Antoniou AC, Consortium BBC, 2017. JAMA 317(23), 2402–2416. [PubMed: 28632866]

Lee JR, Appelmann I, Miething C, Shultz TO, Ruderman D, Kim D, Mallick P, Lowe SW, Wang SX, 2018. Theranostics 8(5), 1389–1398. [PubMed: 29507628]

Lee JR, Bechstein DJB, Ooi CC, Patel A, Gaster RS, Ng E, Gonzalez LC, Wang SX, 2016. Nat Commun 7, 12220. [PubMed: 27447090]

Li JW, Jobichen C, Machida S, Meng S, Read RJ, Chen HY, Jian S, Yuan YA, Sivaraman J, 2023. PLoS Biol 21(3), e3002023. [PubMed: 36917574]

McClarin JA, Frederick CA, Wang B-C, Greene P, Boyer HW, Grable J, Rosenberg JM, 1986. Science 234(4783), 1526–1541. [PubMed: 3024321]

Pingoud A, Jeltsch A, 1997. Eur J Biochem 246(1), 1–22. [PubMed: 9210460]

Pingoud A, Wilson GG, Wende W, 2014. Nucleic Acids Res 42(12), 7489–7527. [PubMed: 24878924]

Pingoud V, Wende W, Friedhoff P, Reuter M, Alves J, Jeltsch A, Mones L, Fuxreiter M, Pingoud A, 2009. J Mol Biol 393(1), 140–160. [PubMed: 19682999]

Polisky B, Greene P, Garfin DE, McCarthy BJ, Goodman HM, Boyer HW, 1975. P Natl Acad Sci USA 72(9), 3310–3314.

Ramachandran A, Santiago JG, 2021. Anal Chem 93(20), 7456–7464. [PubMed: 33979119]

Rananaware SR, Vesco EK, Shoemaker GM, Anekar SS, Sandoval LSW, Meister KS, Macaluso NC, Nguyen LT, Jain PK, 2023. Nat Commun 14(1), 5409. [PubMed: 37669948]

Roh YH, Lee CY, Lee SJ, Kim H, Ly A, Castro CM, Cheon J, Lee JH, Lee H, 2023. Adv Sci 10(10), 2206872.

Terry B, Jack W, Rubin R, Modrich P, 1983. J Biol Chem 258(16), 9820–9825. [PubMed: 6309785]

Thielking V, Alves J, Fliess A, Maass G, Pingoud A, 1990. Biochemistry 29(19), 4682–4691. [PubMed: 2372551]

van Haasteren J, Li J, Scheideler OJ, Murthy N, Schaffer DV, 2020. Nat Biotechnol 38(7), 845–855. [PubMed: 32601435]

Wang W, Wang Y, Tu L, Feng Y, Klein T, Wang J-P, 2014. Sci Rep 4(1), 5716. [PubMed: 25043673]

Woodhead JL, Bhave N, Malcolm AD, 1981. Eur J Biochem 115(2), 293–296. [PubMed: 6263625]

Wright DJ, Jack WE, Modrich P, 1999. J Biol Chem 274(45), 31896–31902. [PubMed: 10542216]

Wurth C, Grabolle M, Pauli J, Spieles M, Resch-Genger U, 2013. Nat Protoc 8(8), 1535–1550. [PubMed: 23868072]

Xu QK, Schlabach MR, Hannon GJ, Elledge SJ, 2009. P Natl Acad Sci USA 106(7), 2289–2294.

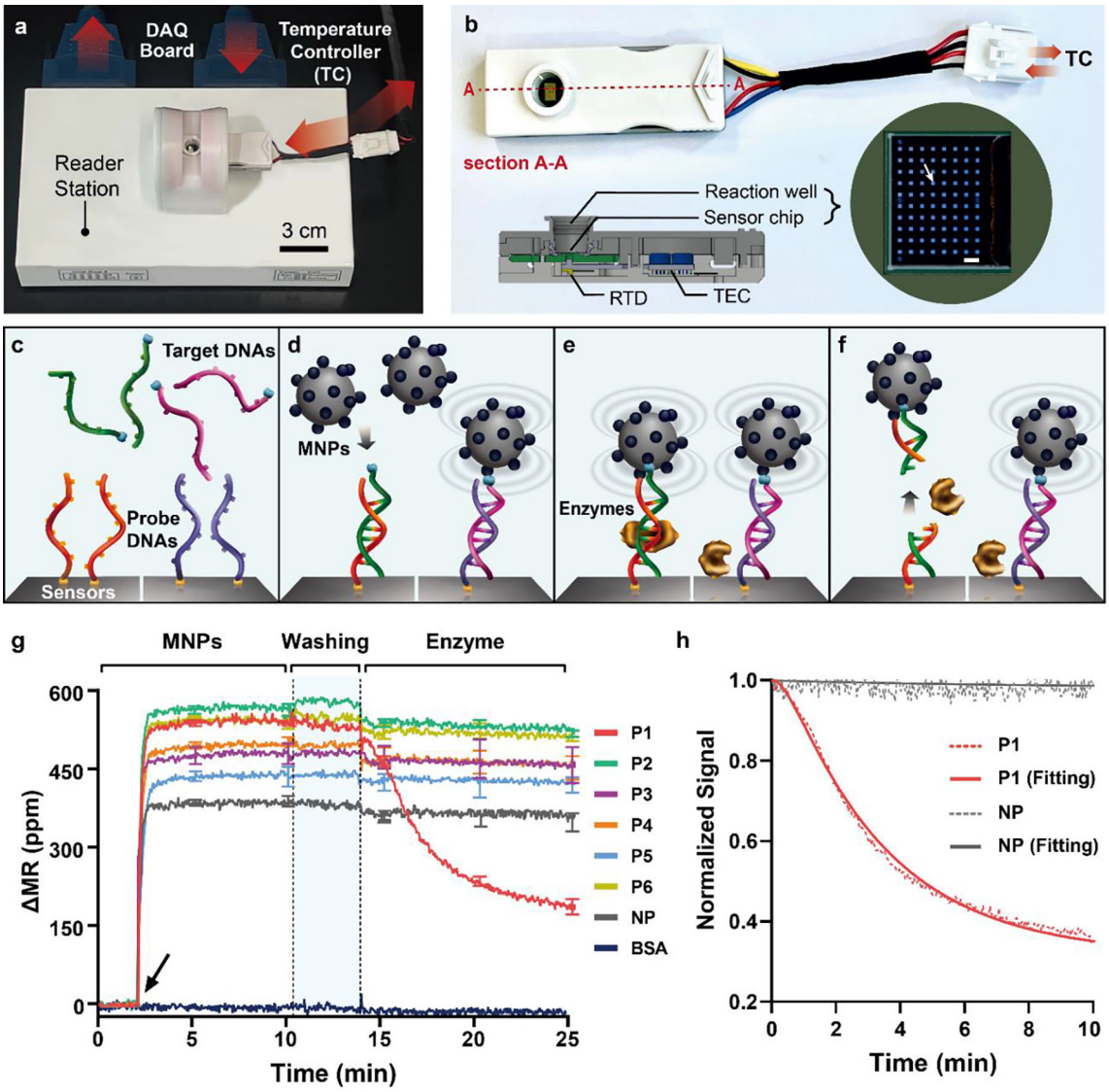

Fig. 1.

(**a**) A custom-made reader station. (**b**) A cross-sectional view of the custom-made cartridge shows integrated RTD and TEC. The arrow indicates an individual sensor, and the scale bar is 500 μm. (**c**) Biotinylated target DNAs were added to the reaction well and hybridized with respective probe DNAs immobilized on different sensors. (**d**) MNPs were added to the reaction well and bound to hybrids. (**e**) An enzyme-containing solution was added to the chip. (**f**) Sequence-specific hybrids were cleaved by enzymes, and MNPs were released from the surface. (**g**) An example of real-time signals from the sensors functionalized with different probe DNAs (P1– P6, and NP) and BSA. The arrow indicates the addition of MNPs to the chip. After incubation with MNPs (labeled as MNPs), the chip was washed (Washing) and the enzyme-containing solution was then added (Enzyme). The error bars represent the SD of three identical sensors acting as technical replicates (n = 3). (**h**) An example of curve fitting with enzyme-cleaving signals from sensors for P1 and NP. The dotted lines represent

the measured signals and the solid lines represent the curves fitted using a mathematical model.

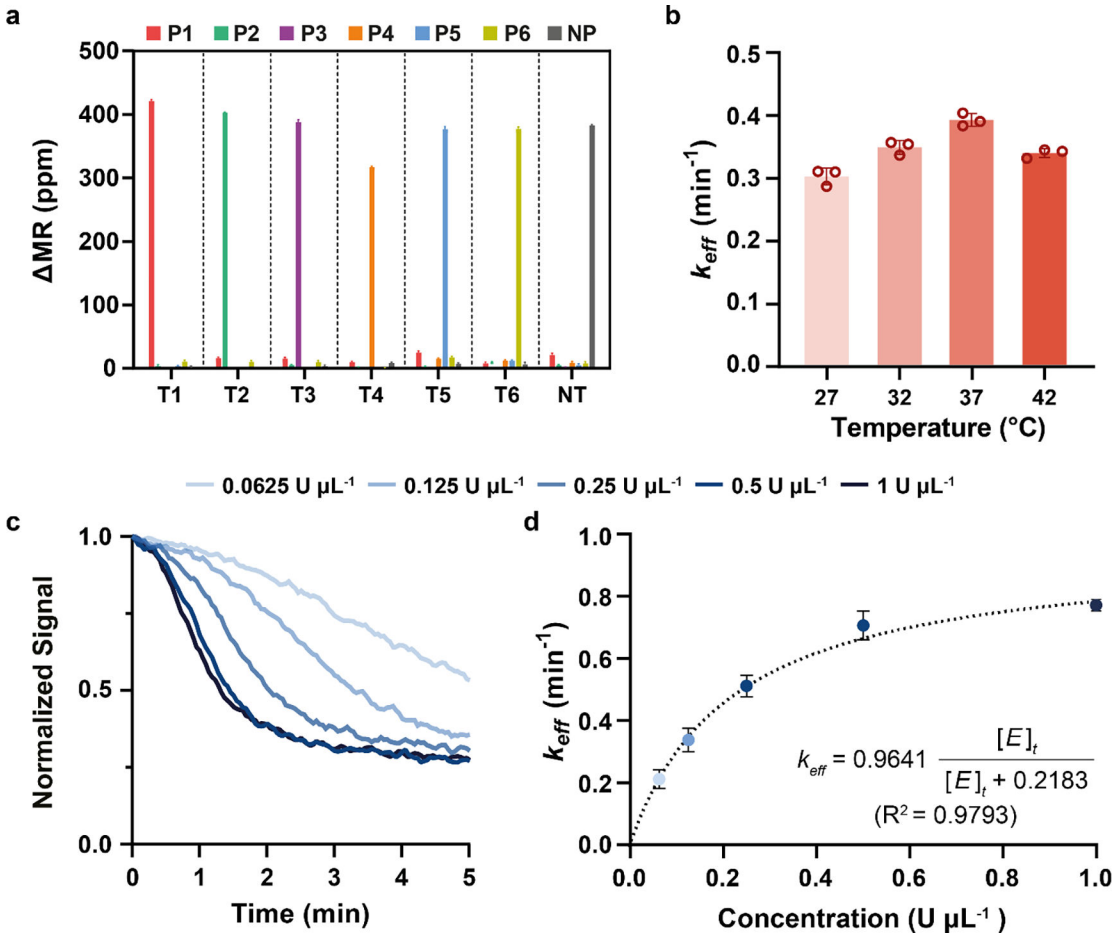

Fig. 2.

(**a**) Cross-reactivity test between each target DNA and its complementary and non-complementary probe DNAs. (**b**) Effective cleavage rates of EcoRI at 1 U μL^{-1} versus temperature. The bar graphs represent the average ± SD of three identical sensors (n = 3). (**c**) Real-time normalized cleavage curves at five different concentrations of EcoRI at 37 °C. These curves represent the average signals of three identical sensors. (**d**) Effective cleavage rates versus concentrations of EcoRI obtained using the normalized cleavage curves. The error bars represent the SD of three identical sensors (n = 3). The dotted line is the curve fitted using equation (2).

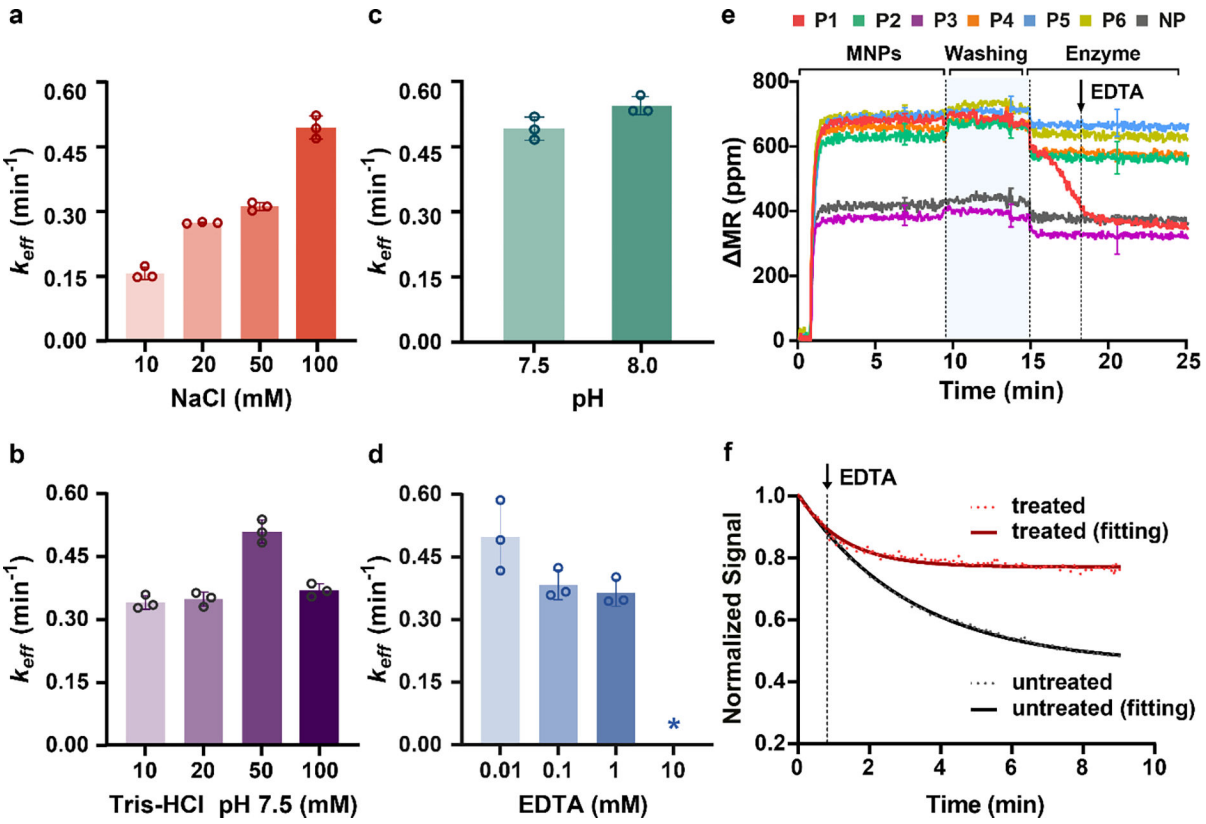

Fig. 3.

Effective cleavage rate versus (**a**) NaCl concentration, (**b**) Tris-HCl (pH 7.5) concentration, (**c**) pH, and (**d**) EDTA concentration. The bar graphs represent the average ± SD of three identical sensors (n = 3). An asterisk indicates that no measurable effective cleavage rate was detected. (**e**) Real-time signals with addition of EDTA in the course of an enzymatic reaction with EcoRI at 0.25 U μL^{-1}. An arrow with EDTA indicates the addition of EDTA to the chip. The error bars represent SD of three identical sensors (n = 3). (**f**) Normalized cleavage curves (dotted lines) and fitted curves (solid lines) for EDTA-treated (red) and untreated (black) reactions.

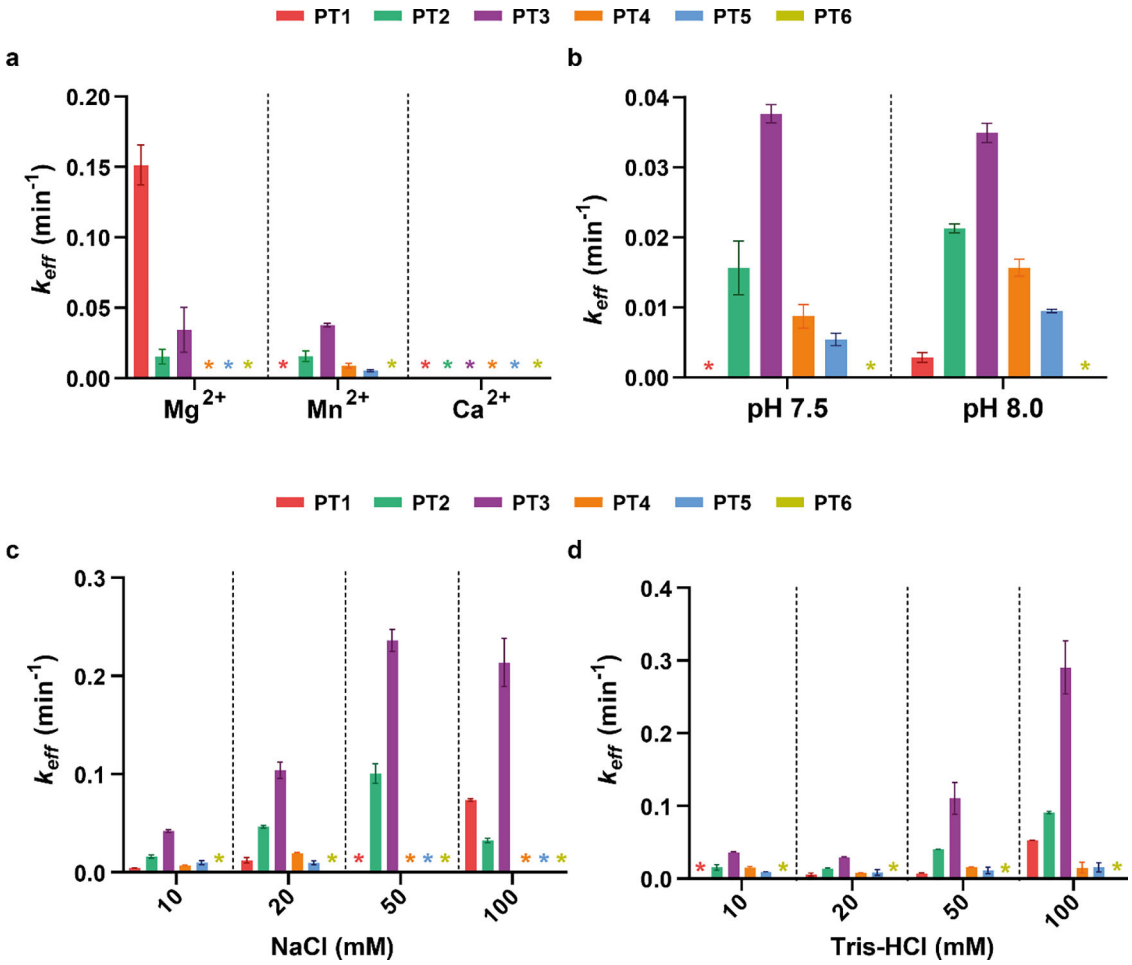

Fig. 4.

(**a**) Effective cleavage rates of EcoRI for canonical (PT1) and non-canonical (PT2 to PT6) sequences in the presence of different divalent metal ions (Mg^{2+}, Mn^{2+}, and Ca^{2+}). (**b**) Sequence-dependent star activity of EcoRI at pH 7.5 and 8.0 in Mn^{2+}-based buffers. (**c**) The effect of salinity on the star activity of EcoRI. (**d**) The effect of ionic strength on star activity. The bar graphs represent the average ± SD of three identical sensors (n = 3). Asterisks indicate that the effective cleavage rate was negligible.

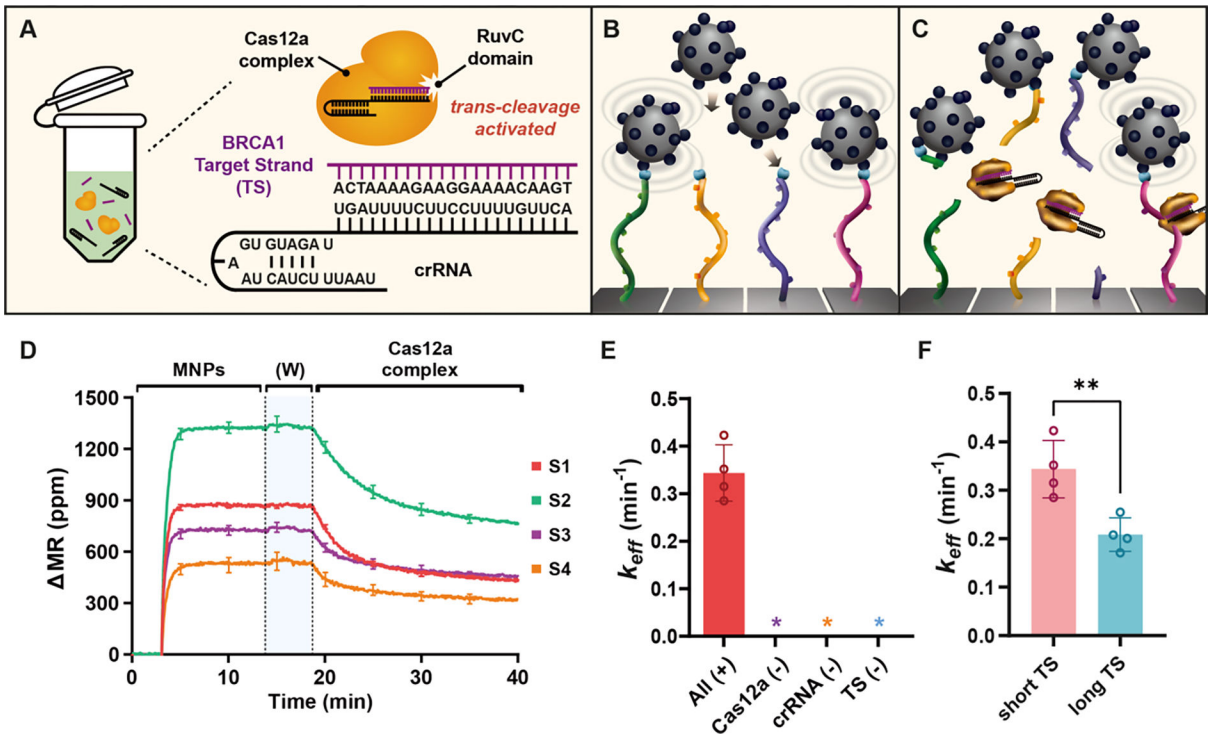

Fig. 5.

(**a**) Assembly of the Cas12a complex. (**b**) MNPs were conjugated with biotinylated ssDNAs immobilized on the sensors. (**c**) Activated Cas12a complexes were then introduced, and biotinylated oligonucleotides were cleaved by the complexes. (**d**) An example of real-time signals produced by the Cas12a assay. MNPs were first introduced, and the sensors were washed (W). Cleavage signals were then generated after the Cas12a complexes were added. The error bars represent the SD of three identical sensors (n = 3). (**e**) Effective cleavage rates of Cas12a with all components or with one missing component. The bar graph represents the average ± SD of four different kinds of biotinylated oligonucleotides with triplicates (n = 4). Asterisks indicate that the effective cleavage rates were negligible. (**f**) Effect of the TS length. The bar graphs represent the average ± SD of four different kinds of biotinylated oligonucleotides with triplicates (n = 4). A Mann–Whitney U test (two-tailed) was performed, and ** indicates $p < 0.01$.